Along-track resolution enhancement for bistatic SAR imaging in burst-mode operation

Virginie Kubica, Xavier Neyt, *Member, IEEE,* and Hugh Griffiths, *Fellow, IEEE*

***Abstract*—Wide-swath SAR imaging modes such as ScanSAR or TOPSAR share the synthetic aperture length between beam positions. This leads to a degraded along-track resolution compared to the conventional Stripmap mode. We show that this degraded resolution can be enhanced in the case of a bistatic configuration by exploiting the sidelobe emissions of the elevation beams illuminating the adjacent sub-swaths. If the SNR of the backscattered signals is sufficient, the performance of the Stripmap mode can even be restored. This concept becomes particularly useful when spaceborne illuminators of opportunity are considered. Indeed, the imaging mode of spaceborne SAR instruments is most often a wide-swath mode. Making it possible to exploit those modes to produce images with high azimuthal resolution dramatically increases the number of useful images that can be produced using emitters of opportunity. Signals from any radar satellite in the receiving band of the receiver can be used, thus further decreasing the revisit time of the area of interest.**

This paper proposes a cross-range resolution-enhancement method which provides an enhanced cross-range resolution compared to the one obtained by the classical burst-mode SAR processing. This method is experimentally validated using measurements acquired in a space-ground bistatic configuration.

***Index Terms*—bistatic radar, matched filter, maximum a posteriori, opportunistic, SAR focusing, ScanSAR, TOPSAR.**

I. Introduction

MOST Synthetic Aperture Radar (SAR) systems can operate in several imaging modes, such as Stripmap, Spotlight, ScanSAR or TOPSAR (Terrain Observation by Progressive Scan SAR) [1], [2] mode. The latter two modes are burst-mode where the antenna is steered in elevation to scan different sub-swaths leading to a discontinuous mainlobe illumination in azimuth. This allows larger swaths to be imaged (e.g. for global monitoring) at the expense of a degraded cross-range resolution [3]. While in the ScanSAR mode the antenna is steered only in elevation, in TOPSAR mode the antenna is steered in both azimuth and elevation. For comparison purpose with the existing literature, the theory developed in this paper is illustrated with ScanSAR illuminations but can easily be extended to TOPSAR illuminations.

A classical way to focus ScanSAR data [4] is to process each burst independently. If the area of interest is illuminated by a number of bursts N_L, the focused burst images can be added incoherently for the purpose of speckle reduction. This single-burst processing results in the well-known poor cross-range resolution of the ScanSAR mode. One way to improve this cross-range resolution is to process coherently the N_L bursts yielding a single-look image. In this case, azimuthal grating lobes appear in the SAR image [5], [6] due to the gaps in the azimuthal phase history. Now, if the Signal-to-Noise Ratio (SNR) of the backscatttered signals resulting from the elevation sidelobes of the other beams is sufficient, a continuous illumination of the scene occurs. Focusing all contiguous bursts will improve the cross-range resolution compared to that obtained by focusing a single-burst and will reduce the undesirable grating lobes. To further improve the performance, we propose a cross-range resolution-enhancement method which can further reduce the grating lobes resulting in the same performance as in the Stripmap mode.

Since the Elevation Antenna Pattern (EAP) of a spaceborne SAR transmitter is shaped in such a way that echoes from scatterers located at ambiguous ranges are suppressed [7], [8], the two-way attenuation makes it difficult to obtain a signal of sufficient SNR in the elevation sidelobes. This attenuation is less of an issue when a bistatic configuration is considered in which the receiving antenna is constantly pointed towards the area of interest. The receiving antenna pattern can then be shaped to suppress the echoes from ambiguous ranges. Bistatic SAR (BSAR) is not new and has been conducted in air-air [9], [10], air-space [11], space-space [12], [13], air-ground [14] or space-ground [15]–[18] configurations. However, the concept of improving the resolution of low-resolution mode makes sense when spaceborne emitters of opportunity are considered. Indeed, the imaging mode of spaceborne SAR instruments is most often a wide-swath mode [19]. Making it possible to exploit those modes to produce images with high azimuthal resolution dramatically increases the number of useful images that can be produced using emitters of opportunity [20]. Of course cooperative operation could be considered, such that the SAR system would operate in Stripmap mode and thus would make high azimuthal resolution possible. That would however likely conflict with the needs of other users. Since emitters of opportunity are considered, signals from any radar satellite in the receiving band of the receiver can be used, thus further decreasing the revisit time of the area of interest. The research community in BSAR imaging mostly limit their analysis to the conventional Stripmap mode [9], [10], [15]–[18]. Examining burst-mode illumination in a bistatic configuration for high-resolution imaging purposes appears to be the first study of its kind.

The paper is organized as follows. Section II describes

V. Kubica is with the Electrical Engineering Department at the Royal Military Academy, Brussels, Belgium and is a Ph.D. student at University College London (e-mail: virginie.kubica@rma.ac.be).

X. Neyt is with the Electrical Engineering Department at the Royal Military Academy, Brussels, Belgium (e-mail: xavier.neyt@rma.ac.be).

H. Griffiths is with the Department of Electronic and Electrical Engineering at University College London, UK (e-mail: hugh.griffiths@ucl.ac.uk).

the bistatic geometry. Our main contribution can be found in Section III where a novel cross-range resolution-enhancement method is proposed to deal with burst-mode illumination. One drawback of the cross-range resolution-enhancement method is the increase of the noise content in the SAR image, the impact of which is experimentally analyzed in Section IV. Finally, Section V concludes the paper.

II. Wide-swath modes in bistatic operation

Although many bistatic configurations can be considered, Fig. 1 illustrates the bistatic configuration of the experiments. In that configuration, a stationary receiver on the roof of a building is used for practical experimental reasons, but the method and the developments that follow are generic. The backscattering geometry, in which the observed area is on the extended baseline transmitter-receiver, is considered. This corresponds to a bistatic angle close to zero and yields the best bistatic slant-range resolution [17]. ScanSAR obtains wide-swath coverage by periodically switching the antenna elevation beam to illuminate several range sub-swaths. A SAR system with three looks and four sub-swaths is shown in Fig. 1. Each sub-swath is illuminated by the antenna beam for a short time interval, T_B, called burst duration, with a T_R periodicity.

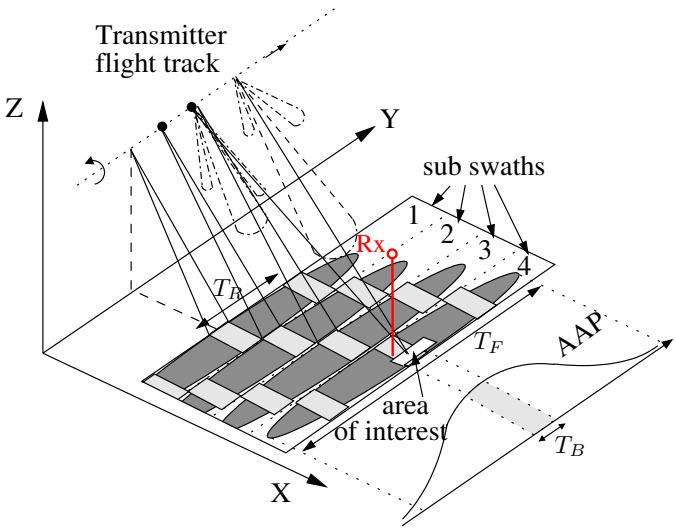

Fig. 1. Bistatic acquisition geometry in the ScanSAR imaging mode. T_B is the burst duration, T_R the scan-repeat time and T_F the antenna-footprint time. The observed area of interest is located at the edge of the global swath and is illuminated by the elevation sidelobes of the beam illuminating sub-swath 3 and afterwards, by the mainlobe illuminating sub-swath 4.

The receiving system (Rx) is located in such a way that the SNR of the backscattered signals coming from the scatterers illuminated by the elevation sidelobes of the transmitter is adequate. The one-way Azimuth Antenna Pattern (AAP) of the transmitter, represented on the right in Fig. 1 as a bell-shape, is fixed in azimuth. Consequently, targets at different azimuths are illuminated by different portions of the AAP of the transmitter.

Figure 2 shows the amplitude modulation function for two different ScanSAR passes of the European Space Agency's (ESA) ENVISAT satellite [21] in Wide Swath (WS) mode over Brussels, Belgium. If the scatterer is at the very edge

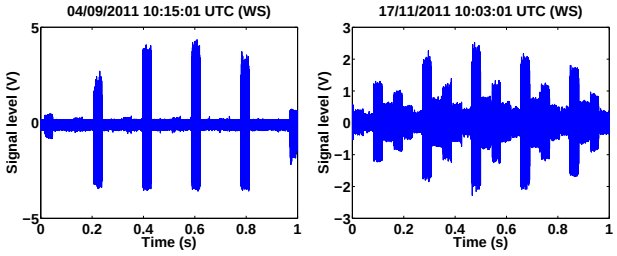

Fig. 2. Acquired ENVISAT's signals in Wide Swath mode: (a) single-beam illumination and (b) five-beam illumination.

of the global swath, only one beam will be received during the along-track illumination as shown in Fig. 2 (a), leading to gaps in the along-track direction. The signals coming from the beams illuminating the other sub-swaths are barely visible. However, if the scatterer is in the center of the global swath, reception of signals from all five elevation beams is possible as shown in Fig. 2 (b). The amplitude of the transmitted pulses in both acquisitions is obviously determined by the combined AAP of the transmitting and the receiving antennas but also, for each beam, by the corresponding EAP at the elevation angle at which the scatterer is located. The amplitude modulation experienced by the scatterers can be estimated based on the geometry. However, if the receiver is close to the area of interest, the amplitude modulation as seen by the scatterers also applies to the direct signal. In that case, the amplitude modulation can be estimated based on the direct signal measurements.

III. Cross-range resolution-enhancement method

In this section, a generic SAR model is first presented. Then, starting from the optimal SAR focusing, we propose a method to recover the Stripmap performance in the case of a ScanSAR illumination. We then assess the performance of this cross-range resolution-enhancement method based on real measurements.

A. SAR signal model

Let us consider a bistatic geometry with a transmitter operating in ScanSAR mode. We consider here the unidimensional case for simplicity and K ground patches along a bistatic isorange contour. If Range Cell Migration (RCM) is negligible, the measured range-compressed data corresponding to the considered range bin can be written as a column vector, $\mathbf{y^k} \in \mathbb{C}^{\mathbf{M\times 1}}$, with M being the number of transmitted pulses. The received data due to the k^{th} ground patch can be modeled as

$$\mathbf{y^k} = \mathbf{W}\mathbf{h^k}x^k + \mathbf{n} \tag{1}$$

where x^k is the complex reflectivity of the k^{th} ground patch and $\mathbf{n} \in \mathbb{C}^{M\times 1}$ denotes the thermal noise. The column vector $\mathbf{h^k} \in \mathbb{C}^{M\times 1}$ represents a received signal if a scatterer at patch k has a reflectivity of 1 and includes the AAP weighting of the transmitting and the receiving antennas. This

AAP weighting depends on the location of the target in the observed area. In addition to the AAP weighting embedded in $\mathbf{h^k}$, the received signals undergo a slow-time amplitude modulation represented by $\mathbf{W} = diag(\mathbf{w})$ with $\mathbf{w} \in \mathbb{R}^{M\times 1}$. This modulation function is determined, for each beam, by the corresponding elevation antenna gain at the elevation angle at which the scatterer is located. The model in (1) assumes an invariant $\mathbf{W}$ along the considered bistatic isorange contour. The validity of this assumption will limit the size of the area that can be imaged according to its position with respect to the transmitter and the receiver. $\mathbf{W}$ depends on the elevation angle under which the scatterers are illuminated by the transmitter. Thus, if the transmitter flies along a straight path, the scatterers located along a line parallel to the transmitter flight path will be subject to the same $\mathbf{W}$. In the case of the Advanced Synthetic Aperture Radar (ASAR) antenna of ENVISAT, and if a difference of 0.25 dB in $\mathbf{W}$, which corresponds to the specified one-way antenna calibration error [22], is accepted, the bistatic isorange may deviate from the above-mentioned straight line by up to 20 km.

The total received signal seen by the radar is then the sum of the responses from all ground patches along one isorange contour and can be modeled as

$$\mathbf{y} = \mathbf{WHx} + \mathbf{n} = \mathbf{H_w x} + \mathbf{n} \tag{2}$$

with $\mathbf{x} = [x^0, x^1, ..., x^k, ..., x^{K-1}]^T$ and $\mathbf{H} = [\mathbf{h^0}, \mathbf{h^1}, ..., \mathbf{h^k}, ..., \mathbf{h^{K-1}}]$.

B. Bistatic ScanSAR focusing

The SAR image formation problem involves reconstruction of the target reflectivity function $\mathbf{x}$ from the measurements $\mathbf{y}$. The unknown reflectivity vector $\mathbf{x}$ can be estimated by maximizing its *a posteriori* probability density function (PDF) or

$$\hat{\mathbf{x}} = \arg\max_{\mathbf{x}} p(\mathbf{x}|\mathbf{y}). \tag{3}$$

Assuming a complex Gaussian distributed reflectivity [23] and Gaussian noise, it is easily shown that the maximum is reached for [24]

$$\hat{\mathbf{x}} = \mathbf{H_r^\dagger y} \tag{4}$$

with

$$\mathbf{H_r^\dagger} = \mathbf{R_x H_w^\dagger}(\mathbf{H_w R_x H_w^\dagger} + \mathbf{R_n})^{-1} \tag{5}$$

where $\mathbf{R_x} = E[\mathbf{x}\mathbf{x}^\dagger]$ is the covariance matrix of the scene reflectivity $\mathbf{x}$ and $\mathbf{R_n}$ is that of the noise $\mathbf{n}$. Note that the Maximum A Posteriori (MAP) estimator (5) is identical to the Minimum Mean Square Error (MMSE) estimator [25] in the Gaussian signal model.

The computation of (5) is feasible in the classical single-burst processing [4]. However, in a continuous illumination case, (5) is computationally demanding and another implementation is now discussed.

If $\mathbf{x}$ and $\mathbf{n}$ are samples of Gaussian stationary processes and the elements of the vectors $\mathbf{x}$ and $\mathbf{n}$ are assumed uncorrelated, then the covariance matrices become $\mathbf{R_x} = \sigma_x^2\mathbf{I}$ and $\mathbf{R_n} = \sigma_n^2\mathbf{I}$ with σ_x^2 and σ_n^2 respectively the variance of the scene reflectivity and the noise and $\mathbf{I}$ the identity matrix. The optimum focusing (5) simplifies thus as

$$\begin{aligned}\mathbf{H_r^\dagger} &= \mathbf{H_w^\dagger}(\mathbf{H_w H_w^\dagger} + \vartheta\mathbf{I})^{-1} \\ &= \mathbf{H^\dagger}[\mathbf{W}^\dagger(\mathbf{WHH}^\dagger\mathbf{W}^\dagger + \vartheta\mathbf{I})^{-1}]\end{aligned} \tag{6}$$

where $\vartheta = \frac{\sigma_n^2}{\sigma_x^2}$ is the inverse of the SNR.
If the conditions to have $\mathbf{HH}^\dagger$ diagonal are met, the matrix operation in brackets in (6) is simply a multiplication between diagonal matrices which leads to

$$\mathbf{H_r^\dagger} = \mathbf{H^\dagger C_w} \tag{7}$$

where the matrix $\mathbf{C_w}$ is a diagonal matrix with the diagonal elements equal to

$$c_{w,i} = \frac{w_i}{w_i^2 K + \vartheta} \tag{8}$$

with w_i the i^{th} element of $\mathbf{w}$. This matrix acts as a compensation of the slow-time modulation embodied by $\mathbf{w}$, or in another words, restore the performance degraded by the multiplication by $\mathbf{W}$ in (2). This equation holds if $\mathbf{HH}^\dagger$ is diagonal which is achieved if the ground patches are resolved.

Finally, the SAR focusing (4) simplifies in

$$\hat{\mathbf{x}} = \mathbf{H^\dagger C_w y} \tag{9}$$

This result implies that the cross-range resolution-enhancement method consists in

- compensating in the measurement domain, the slow-time modulation of the measurements induced by the beam scanning in elevation

$$\mathbf{y_c} = \mathbf{C_w y} \tag{10}$$

- focusing using the conventional Matched Filter (MF)

$$\hat{\mathbf{x}} = \mathbf{H^\dagger y_c} \tag{11}$$

C. Performance analysis

In this section, the performance of (9) are evaluated based on real ScanSAR measurements. We considered the ASAR instrument of ENVISAT as source, but the results can easily be extended to other transmitters. ScanSAR focusing using (9) depends on the slow-time amplitude modulation $\mathbf{w}$ which in turn depends on the position of the imaged area of interest in the global swath. This can be parametrized using the elevation angle at which the scatterers are located, denoted θ_{el}. This key parameter can predict whether or not the opportunistic ScanSAR pass is suitable for the use of the cross-range resolution-enhancement method (9). To predict the performance, the elevation antenna diagram of the transmitted beams of the opportunistic transmitter must be measured. As ESA provides the two-way elevation diagram of the 5 elevation beams of the ASAR instrument of ENVISAT for 5° around the beam centre, data acquired over six months by the stationary ground-based receiver were used to complement the elevation diagrams at other angles. Figure 3 depicts the ESA calibrated amplitude elevation diagrams of the five beams of ASAR used in ScanSAR mode (solid lines) and the extrapolation (dashed lines) based on our measurements (dots).

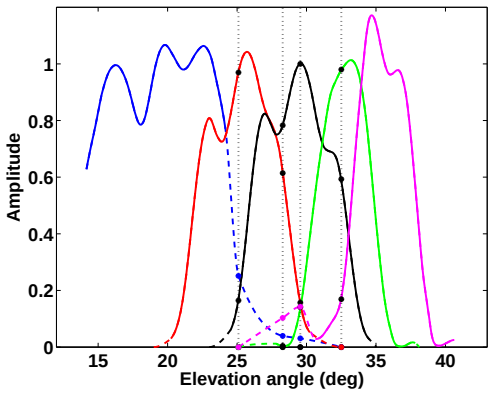

Fig. 3. Extrapolated antenna elevation diagrams of the 5 beams of the ASAR antenna. The dots on the dashed line denote our measurements and the dots on the solid line denote the values obtained from sampling antenna patterns provided by ESA.

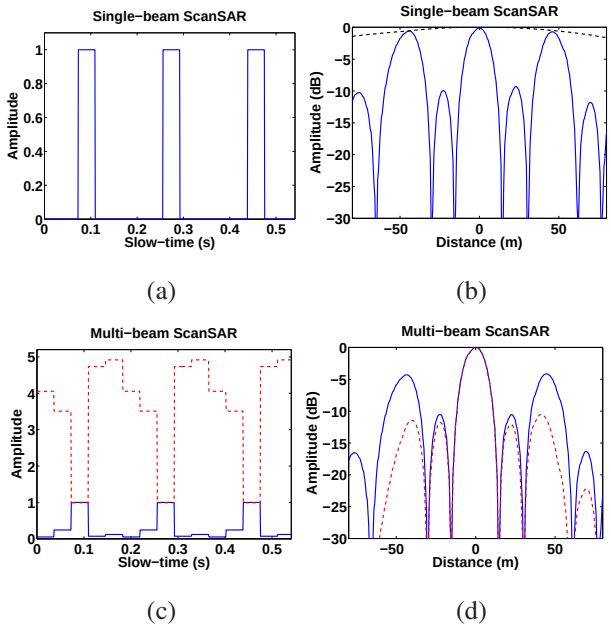

Fig. 4. On the left, the normalized slow-time amplitude modulation $\mathbf{w}$ of two extreme ScanSAR illuminations, and on the right, cuts of the IRF along the scatterer's isorange.

To give a quantitative insight of the performance of the method, a simulation of a point scatterer in presence of noise is performed. A SNR of -10 dB before any coherent processing is simulated and two extreme situations are envisaged. First, a single-beam ScanSAR illumination, as would be obtained for a scatterer at the very edge of the wide swath is considered. This case could correspond for instance to $\theta_{el} = 15°$ in Fig. 3. This geometry would result in a pulse-train window modulation $\mathbf{w}$ as illustrated in Fig. 4 (a). Figure 4 (b) represents the intensity of the azimuthal Impulse Response Function (IRF) obtained if one single burst is focused (dashed line) and if all bursts are coherently processed (solid line) using a conventional MF. The latter drastically improves the poor resolution of the single-burst processing but grating lobes appear.

When the scatterer is ideally situated, i.e. at the centre of the global swath ($\theta_{el} = 29°$ in Fig. 3), reception of signals from all five elevation beams is possible but each with a different amplitude according to the elevation antenna diagram of the considered beam as shown in Fig. 4 (c) (solid line). In this case, the aforementioned gaps are filled by the sidelobes emission of the transmit antenna leading to a reduction of the amplitude of the grating lobes as shown in Fig. 4 (d) (solid line). The PSLR improved from 0.5 dB for a single-beam illumination to 4 dB for a multi-beam illumination. That demonstrates that gap-filling is a step in the right direction to approach the Stripmap performance.

By applying the cross-range resolution-enhancement method (9), the residual grating lobes due to the ScanSAR data are attenuated by about 8 dB which puts it at the same level as the other sidelobes as illustrated in Fig. 4 (d) (dashed line). That will be the case if the SNR of the backscattered signals coming from the scatterers illuminated by the elevation sidelobes of the transmitting antenna is sufficient. The applied weighting function $\mathbf{c_w}$ is shown in Fig. 4 (c) (dashed line). It is obvious that the product $c_{w,i}w_i$ for $i = 0 \dots M-1$ must converge to 1 to approach the PSLR of the Stripmap mode. This will happen for very small ϑ, i.e. very large SNR.

It is important to stress that the grating lobes pattern in the azimuthal IRF depends on the wide-swath mode, i.e. on the number of sub-swaths, N_S, and on the number of looks, N_L, of the SAR mode. Wide-swath modes designed with $N_L > 1$ as is the case for the wide-swath modes of ENVISAT or RADARSAT-2 [26] can give rise to grating lobes in the azimuthal IRF if the N_L bursts are coherently focused. The distance between the mainlobe of the IRF and the first grating lobe is inversely proportional to $N_S W_B$ with W_B the azimuthal burst bandwidth [6]. For a one-look wide-swath mode, such as the TOPSAR mode implemented on Sentinel-1A [19], the azimuthal IRF is not corrupted by grating lobes. In this mode, the proposed method can still recover the Stripmap cross-range resolution as shown in [27]. In any wide-swath imaging illumination, the cross-range resolution-enhancement method provides, under certain conditions, a better cross-range resolution compared to the classical processing of a single burst.

Let us now simulate different satellite passes over $15° \leq \theta_{el} \leq 40°$. Figure 5 (a) shows the computed PSLRs of the IRF for each geometry obtained with the conventional MF (dashed line) and with the conventional MF preceded by the amplitude compensation (9) (solid line). For $27° \leq \theta_{el} \leq 32°$, the PSLR of the MF output with the pre-processing step (10) is by far better than without. For those geometries with small ϑ, $c_{w,i}$ tends to the inverse of w_i, compensating appropriately the slow-time modulation, i.e. leading to a reduction of the grating lobes, but, at the same time, will amplify the noise included in $\mathbf{y}$. Outside that angular range, one or several beams are barely present leading to a poor signal amplitude over part of the aperture (large ϑ). In those cases, $c_{w,i}$ will neither amplify the signal nor the noise: the poor SNR will not degrade but the grating lobes will remain. The noise amplification induced

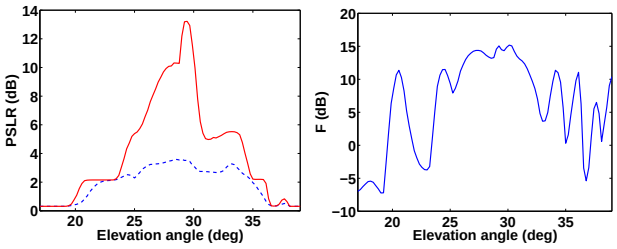

(a) (b)

Fig. 5. (a) Calculated PSLR for different antenna elevation angles without compensation (dashed line) and with compensation (solid line) and (b) calculated relative noise energy (w.r.t. Stripmap mode) amplification due to the compensation method.

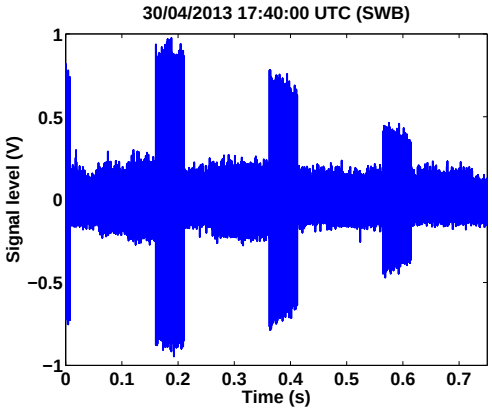

Fig. 6. Signal acquired during an overpass of RADARSAT-2 operating in SWB mode defined by four beams and a burst duration of 0.05 sec.

by the method can be quantified using

$$F = 10\ log_{10}\left(\frac{1}{M}\sum_{i=0}^{M-1}|c_{w,i}|^2\right) \tag{12}$$

This parameter, depicted in Fig. 5 (b), represents the factor by which the noise variance is amplified relative to the constant $\mathbf{W}$ case. The reduction of the grating lobes is accompanied by a noise amplification by up to 15 dB. In the light of the foregoing, it may be concluded that $\mathbf{c_w}$ strives to achieve a trade-off between the compensation of the slow-time modulation, and thus the reduction of the grating lobes, and the amplification of the noise. Note that $\mathbf{c_w}$ minimizes the MSE of the ground reflectivity when ϑ in (8) is the true value, ϑ_{true}. $\mathbf{c_w}$ was not designed to maximize the PSLR. However, choosing a smaller value $\vartheta < \vartheta_{true}$ may yield a larger PSLR at the expense of a larger amplification of the noise.

IV. Results based on real measurements

On the 30^{th} of April 2013, the stationary ground-based receiver, located in Brussels, was in the centre of the swath of the Canadian satellite RADARSAT-2 operating in the ScanSAR Wide mode (SWB). Figure 6 represents the four-beam RF signal acquired during its overpass.

The performance of the cross-range resolution-enhancement method can be illustrated by analyzing a point-like target in the image. Figure 7 (a) shows the intensity of the Single-Look Complex (SLC) SAR image centered on the point scatterer obtained by the classical MF processing of a single burst. This yields a poor resolution of $100m$ in the along-track direction. If the N_L bursts of this same beam are coherently focused, the along-track resolution is drastically improved to $20m$ as shown in Fig. 7 (b). The expected grating lobes in azimuth along the isorange can be observed. Note that a second point scatterer at (Lat, Long)=$(50.8457, 4.3992)$ is hidden in the grating lobes. The white square in the upper right corner of Fig. 7 represents a region assumed free of signals to estimate the background noise level with respect to the single-beam MF case of Fig. 7 (b). The corresponding values are given in Table I.

TABLE I
Noise level estimation relative to the single-beam MF case.

SAR focusing method	Relative noise variance dB
Cross-range resolution-enhancement method for $\vartheta = \vartheta_{true}$ (Fig. 7 (c))	8
Cross-range resolution-enhancement method for $\vartheta < \vartheta_{true}$ (Fig. 7 (d))	16.7

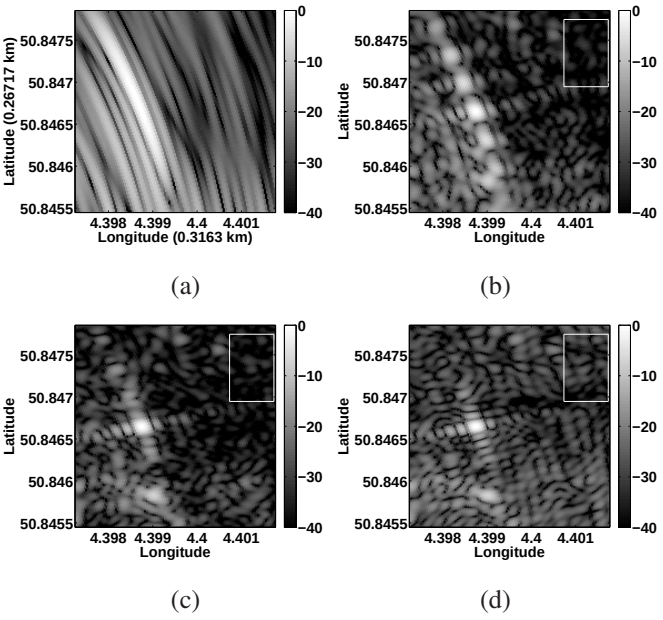

(a) (b) (c) (d)

Fig. 7. Zoom on a point scatterer in the georeferenced SLC SAR image processed using (a) the conventional MF on a single-burst, (b) the conventional MF on a single beam, (c) the cross-range resolution-enhancement method with $\vartheta = \vartheta_{true}$ and (d) with $\vartheta < \vartheta_{true}$.

If the cross-range resolution-enhancement method is applied with the true value ϑ_{true}, there is a tradeoff between the amplification of the noise and the reduction of the grating lobes. The latter are reduced but still present in Fig. 7 (c). The second point scatterer is now visible. For $\vartheta < \vartheta_{true}$, the weighting function $\mathbf{c_w}$ becomes closer to the inverse of $\mathbf{w}$: a better compensation of the slow-time amplitude modulation is obtained at the expense of an increase of the noise content in the SAR image (Fig. 7 (d)). This illustrates that the compensation function $\mathbf{c_w}$ must be calculated with

the correct SNR, ϑ_{true}. This final result demonstrates that the cross-range resolution-enhancement method provides high cross-range resolution SAR images relative to the classical single-burst ScanSAR imaging. Besides, if the MF is preceded by an amplitude compensation weighting function applied in the slow-time domain, the SAR image has reduced grating lobes but an acceptable noise amplification.

V. Conclusion

In this paper, we have demonstrated that, in the case of a bistatic configuration, the poor cross-range resolution of wide-swath mode can be enhanced by exploiting the signal transmitted in the elevation sidelobes. We showed that the SAR focusing of such data simplifies, under reasonable assumptions, in a compensation weighting function preceding any conventional SAR focusing technique.

This method has a significant operational interest in the opportunistic space-ground geometry as it allows to image more frequently a specific area with a high cross-range resolution. This makes the image production independent of any operators provided the illuminator of opportunity transmits. This benefit becomes even more important as several constellations of satellites can be exploited.

Finally, based on real measurements, it has been shown that the increase in noise induced by the method is very limited.

References

[1] F. De Zan and A. Monti Guarnieri, "TOPSAR: Terrain Observation by Progressive Scans," *IEEE Transactions on Geoscience and Remote Sensing*, vol. 44, no. 9, pp. 2352–2360, 2006.

[2] A. Meta, J. Mittermayer, P. Prats, R. Scheiber, and U. Steinbrecher, "TOPS Imaging With TerraSAR-X: Mode Design and Performance Analysis," *IEEE Transactions on Geoscience and Remote Sensing*, vol. 48, no. 2, pp. 759–769, 2010.

[3] A. Currie and M. A. Brown, "Wide-swath SAR," *Proc. Inst. Elec. Eng. F*, vol. 139, no. 2, pp. 123–135, 1992.

[4] A. Monti-Guarnieri and P. Guccione, "Optimal 'focusing' for low resolution ScanSAR," *IEEE Transactions on Geoscience and Remote Sensing*, vol. 39, no. 3, pp. 479–491, 2001.

[5] R. Bamler and M. Eineder, "ScanSAR Processing Using Standard High Precision SAR Algorithms," *IEEE Transactions on Geoscience and Remote Sensing*, vol. 34, pp. 212–218, Jan. 1996.

[6] J. Holzner and R. Bamler, "Burst-mode and ScanSAR interferometry," *IEEE Transactions on Geoscience and Remote Sensing*, vol. 40, no. 9, pp. 1917–1934, 2002.

[7] F. Li and W. Johnson, "Ambiguities in Spaceborne Synthetic Aperture Radar Systems," *IEEE Transactions on Aerospace and Electronic Systems*, vol. 19, no. 3, pp. 389–397, 1983.

[8] R. Moore, J. Claassen, and Y. Lin, "Scanning Spaceborne Synthetic Aperture Radar with Integrated Radiometer," *IEEE Transactions on Aerospace and Electronic Systems*, vol. 17, pp. 410–421, May 1981.

[9] P. Dubois-Fernandez, H. Cantalloube, B. Vaizan, G. Krieger, R. Horn, M. Wendler, and V. Giroux, "ONERA-DLR bistatic SAR campaign: planning, data acquistiton, and first analysis of bistatic scattering behaviour of natural and urban targets," *IEE Proceedings – Radar, Sonar and Navigation*, vol. 153, pp. 214–223, June 2006.

[10] H. Cantalloube, M. Wendler, V. Giroux, P. Dubois-Fernandez, and R. Horn, "A first bistatic airborne SAR interferometry experiment-Preliminary results," in *IEEE Sensor Array and Multichannel Signal Processing Workshop*, 2004.

[11] M. Rodriguez-Cassola, S. V. Baumgartner, G. Krieger, and A. Moreira, "Bistatic TerraSAR-X/F-SAR Spaceborne-Airborne SAR Experiment: Description, Data Processing, and Results," *IEEE Transactions on Geoscience and Remote Sensing*, vol. 48, pp. 781–794, Feb. 2010.

[12] G. Krieger, I. Hajnsek, K. P. Papathanassiou, M. Younis, and A. Moreira, "Interferometric Synthetic Aperture Radar SAR Missions Employing Formation Flying," *Proceedings of the IEEE*, vol. 98, pp. 816–843, May 2010.

[13] N. Gebert, B. Carnicero Dominguez, M. Davidson, M. Diaz Martin, and P. Silvestrin, "SAOCOM-CS - A passive companion to SAOCOM for single-pass L-band SAR interferometry," in *Proc. EUSAR conference*, pp. 1–4, June 2014.

[14] A. Goh, M. Preiss, N. Stacy, and D. Gray, "The Ingara Bistatic SAR Upgrade: First Results," in *IEEE International Radar conference*, pp. 329–334, Sept. 2008.

[15] H. D. Griffiths, C. J. Baker, J. Baubert, N. Kitchen, and M. Treagust, "Bistatic radar using satellite-borne illuminators," in *IEEE International Conference RADAR 02*, (Edinburgh, UK), pp. 1–5, Oct. 2002.

[16] A. P. Whitewood, C. J. Baker, and H. D. Griffiths, "Bistatic Radar Using Spaceborne Illuminator," in *IET International Radar conference*, (Edinburgh, UK), Oct. 2007.

[17] J. Sanz-Marcos, P. Lopez-Decker, J. J. Mallorqui, A. Aguasca, and P. Prats, "SABRINA: A SAR Bistatic Receiver for Interferometric Applications," *IEEE Geoscience and Remote Sensing Letters*, vol. 4, pp. 307–311, Apr. 2007.

[18] L. Maslikowski, P. Samczynski, M. Baczyk, P. Krysik, and K. Kulpa, "Passive bistatic SAR imaging - Challenges and limitations," *IEEE Aerospace and Electronic Systems Magazine*, vol. 29, no. 7, pp. 23–29, 2014.

[19] "ESA's radar observatory mission for GMES operational services," *ESA Special Publication*, no. 1322/1, 2012.

[20] V. Kubica and X. Neyt, "ScanSAR resolution enhancement in bistatic operation," in *IET International Radar Conference*, (Glasgow, UK), Oct. 2012.

[21] Y.-L. Desnos, C. Buck, J. Guijarro, J.-L. Suchail, R. Torres, and E. Attema, "ASAR-ENVISAT's Advanced Synthetic Aperture Radar," *ESA bulletin*, pp. 91–100, May 2000.

[22] M. Zink, "Update on Antenna Elevation Pattern Estimation from Rain Forest Data," in *Proceedings of the ENVISAT Validation Workshop (ESA SP-531)*, (Italy), Dec. 2002.

[23] C. Oliver and S. Quegan, *Understanding Synthetic Aperture Radar Images*. Raleigh, NC: SciTech Publishing, 2004.

[24] H. Van Trees, *Detection, estimation and modulation theory — Part I*. Wiley, 1968.

[25] S. M. Kay, *Fundamentals of statistical signal processing — Estimation theory*. Englewood Cliffs, NJ: Prentice-Hall, 1993.

[26] R. Raney, A. Luscombe, E. Langham, and S. Ahmed, "RADARSAT," *Proceedings of the IEEE*, vol. 79, pp. 839–849, June 1991.

[27] V. Kubica, X. Neyt, and H. Griffiths, "Improved cross-range resolution in TOPSAR imaging using Sentinel-1A in bistatic operation," in *IEEE International Radar Conference*, (Arlington, VA), 2015.

Virginie Kubica received the B.S and M.S. degrees in engineering in Telecommunications from the Royal Military Academy, Brussels in 2005. As a Captain in the Belgian Air Force, she was head of the Radar Section of the Belgian Air Defence Unit till 2009. Since mid-2009, she has been a teaching assistant at the Communication, Information, Systems and Sensors department at the Royal Military Academy. She has served as the Belgian national representative to the NATO Sensors and Electronics Technology group "Advanced Modelling and Systems Applications for Passive Sensors SET-164" and now serves on its extension "Advanced situation-specific modelling and vulnerability mitigation using passive radar technology SET-207".

Virginie Kubica is currently pursuing the Ph.D. degree at University College London in collaboration with the Royal Military Academy in the domain of passive bistatic SAR imaging.

Xavier Neyt received a master in engineering degree (summa cum laude) from the Université Libre de Bruxelles (ULB) in 1994, a postgraduate degree in Signal Processing (summa cum laude) from the Université de Liège (ULg) in 2004 and a PhD in Applied Science from the Royal Military Academy (RMA) and the Université de Liège in 2008. In 1995 he received the Frerichs Award from the ULB and the special IBM grant from the Belgian National Fund for Scientific Research (NFWO). He also serves on the IEEE Aerospace and Electronic Systems Society Radar Systems Panel and he is a member of the ESA/Eumetsat Scatterometer Scientific Advisory Group.

Since then he has been working as research engineer for the Royal Military Academy, Belgium. In 1996-1997 he was visiting scientist at the French aerospace center (ONERA) and in 1999 at the German aerospace centre (DLR). In 1997-1999 he was responsible for the design of the image compression module of the European MSG satellite and in 2000-2007, responsible for the redesign of the ground processing of the scatterometer of the European ERS satellite following its gyroscope anomaly. Since 2008, he is leading the Scatterometer Engineering Support Laboratory for the European Space Agency at the Royal Military Academy.

He is now associate professor at the Communication, Information, Systems and Sensors department of the Royal Military Academy and leading the Radar Signal Processing Research Unit.

Hugh D. Griffiths (M'86-SM'90-F'99) was educated at Hardye's School, Dorchester, U.K., and Keble College, Oxford University, where he received the M.A. degree in physics in 1978. He also received the Ph.D. and D.Sc. (Eng) degrees from the University of London, London, U.K., in 1986 and 2000, respectively.

He holds the THALES/Royal Academy of Engineering Chair of RF Sensors at University College London. From 2006 to 2008, he served as Principal of the Defence College of Management and Technology, at the Defence Academy of the United Kingdom, Shrivenham. From 1982 to 2006, he was with University College London, serving as Head of the Department of Electronic and Electrical Engineering from 2001 to 2006. His research interests include radar sensor systems and signal processing (particularly synthetic aperture radar and bistatic and multistatic radar and sonar) as well as antennas and antenna measurement techniques. He has published over 400 papers and technical articles on these subjects.

Prof. Griffiths received the IERE Lord Brabazon Premium Award in 1984, the IEE Mountbatten and Maxwell Premium Awards in 1996, the IEEE Nathanson Award in 1996, and the IET A F Harvey Research Prize in 2012. He served as President of the IEEE AES Society for 2012-2013, and is Editor-in-Chief of the journal IET Radar, Sonar and Navigation. He is a Fellow of the IET, and in 1997 he was elected to Fellowship of the Royal Academy of Engineering.